Electronic Supplementary Material (ESI) for Physical Chemistry Chemical Physics.

[Supplementary Information]

Intramolecular charge transfer of a push-pull chromophore with restricted internal rotation of electron donor

Sebok Lee, Myungsam Jen, Gisang Lee, Taehyung Jang, and Yoonsoo Pang*

Department of Chemistry, Gwangju Institute of Science and Technology, 123 Cheomdangwagi-ro, Buk-gu, Gwangju 61005, Republic of Korea

Table of contents

*Authors to whom correspondence should be addressed. E-mail: ypang@gist.ac.kr.

1. Molecular structures of push-pull chromophores

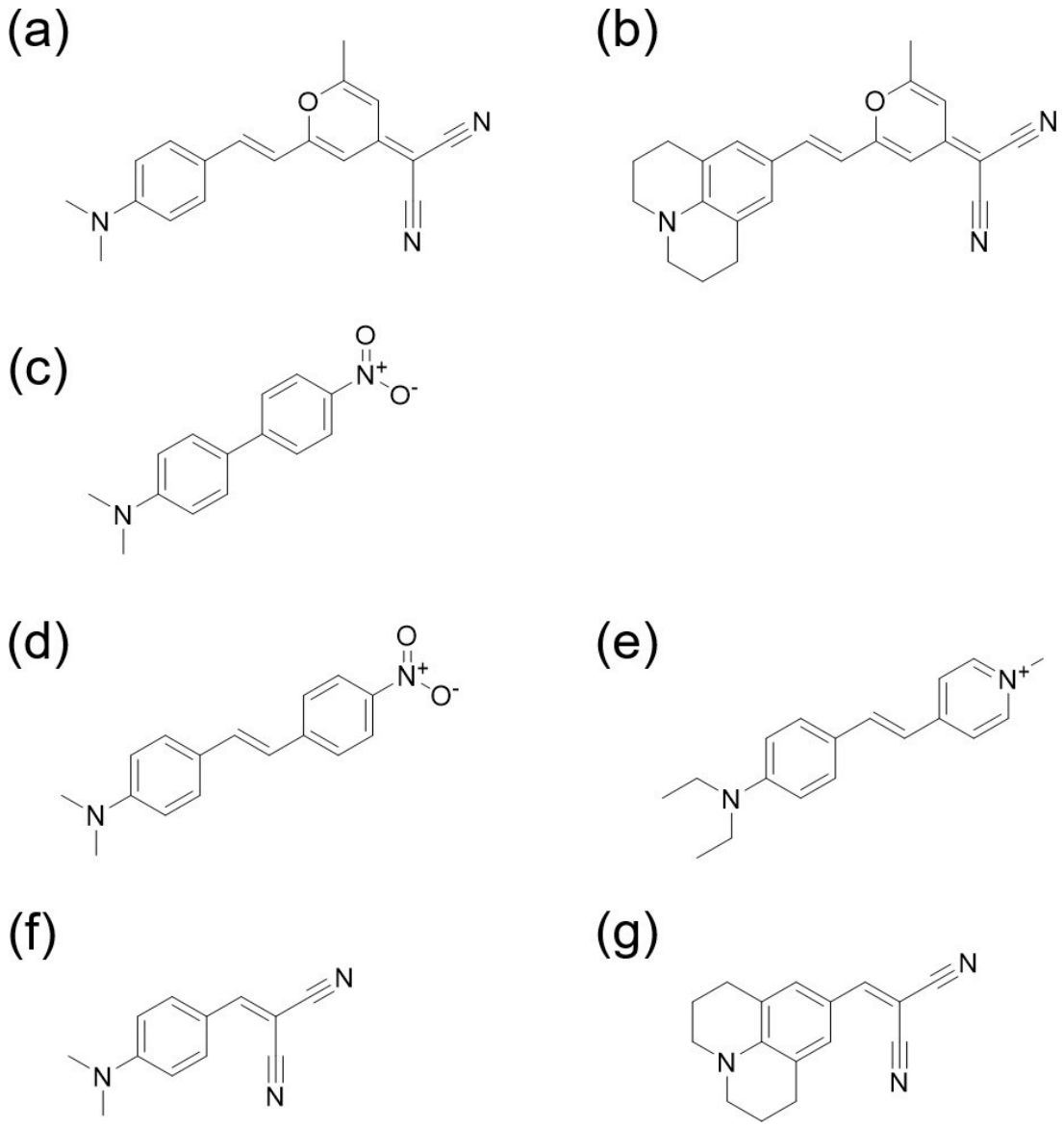

Figure S1. Molecular structures of (a) 4-dicyanomethylene-2-methyl-6-(*p*-dimethylaminostyryl)-4*H*-pyran (DCM), (b) 4-(dicyanomethylene)-2-methyl-6-[2-(2,3,6,7-tetrahydro-1*H*,5*H*-benzo[*ij*] quinolizin-9-yl)vinyl]-4*H*-pyran (LD688), (c) 4-dimethylamino-4′-nitrobiphenyl (DNBP), (d) 4-dimethylamino-4′-nitrostilbene (DNS), (e) 4-*N*,*N*-diethylamino-4 ″ -*N* ′ -methyl-stilbazolium tosylate, (f) 2-(4-(dimethylamino)benzylidene)malononitrile, and (g) 9-(2,2-dicyanovinyl)julolidine.

2. Femtosecond stimulated Raman results of LD688.

The femtosecond stimulated Raman spectra (FSRS) of 4-(dicyanomethylene)-2-methyl-6-[2-(2,3,6,7-tetrahydro-1*H*,5*H*-benzo[*ij*]quinolizin-9-yl)vinyl]-4*H*-pyran (LD688) in DMSO solution with 403 nm excitation are shown in Figure S2. The ground-state Raman spectrum taken at the delay of -5 ps was subtracted from the transient Raman spectra at each time delay between -1 and 100 ps. The background signals as the remnant of the transient absorption spectra were removed by the spectral fit with the low-order polynomial functions (displayed as dotted lines in Figure S2). The difference stimulated Raman spectra of LD688 in DMSO solution, shown in Figure 3(a), were obtained by subtracting the ground-state spectrum from the excited-state Raman spectrum at each time delay.

Figure S3 shows the FSRS of LD688 in $CHCl_3$ obtained with 403 nm excitation, where the ICT does not occur. The ground-state Raman spectrum of LD688 in $CHCl_3$ was similarly subtracted from each excited-state Raman spectrum at a specific delay after the transient absorption backgrounds were removed in the low-order polynomial fits. The difference stimulated Raman spectra of LD688 in $CHCl_3$ solution do not show significant temporal changes and miss the spectral changes in the $\nu_{19b,py}$, $\nu_{8a,ph}$, and $\nu_{C\equiv N,sym}$ modes with the ICT.

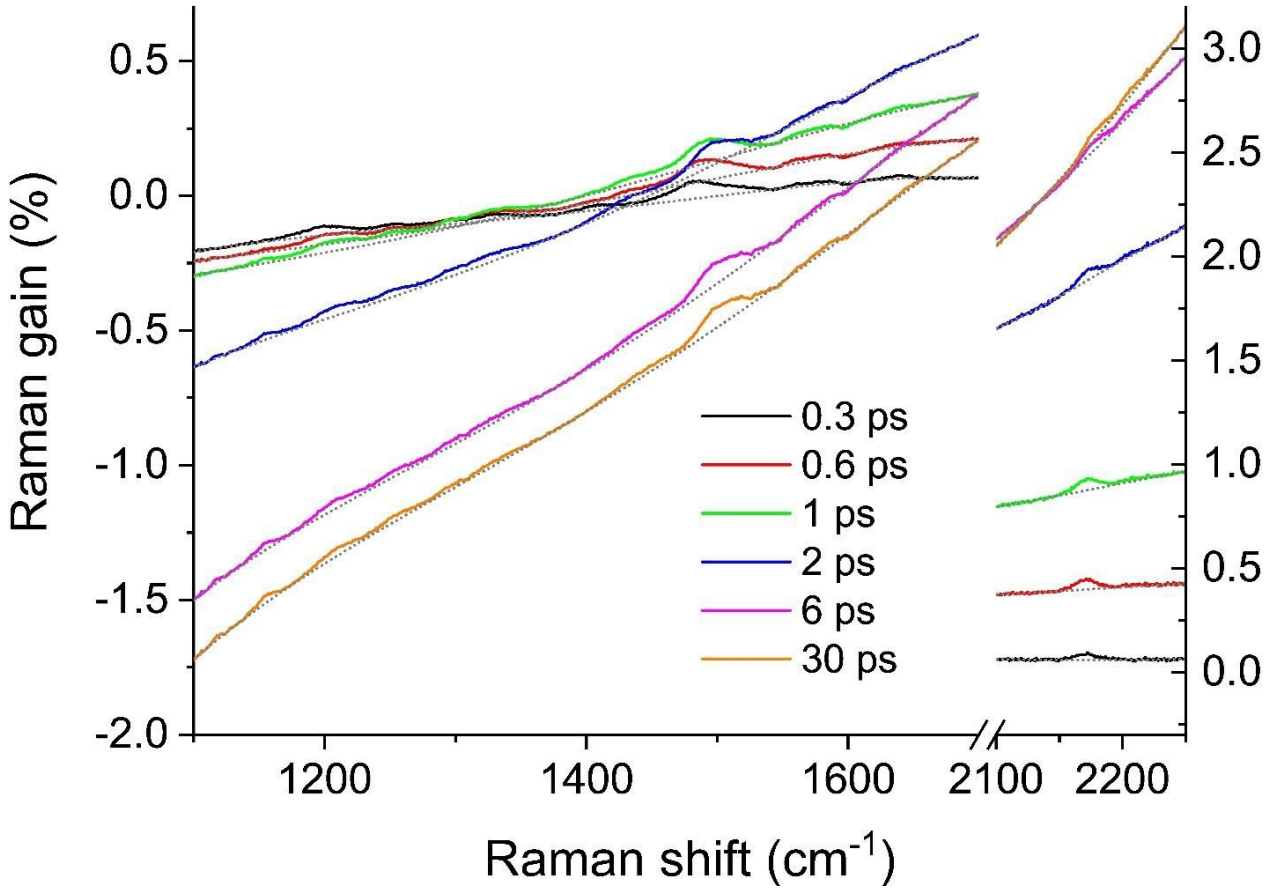

Figure S2. Transient absorption backgrounds were removed by the low-order polynomial functions from the FSRS results of LD688 in DMSO with 403 nm excitation.

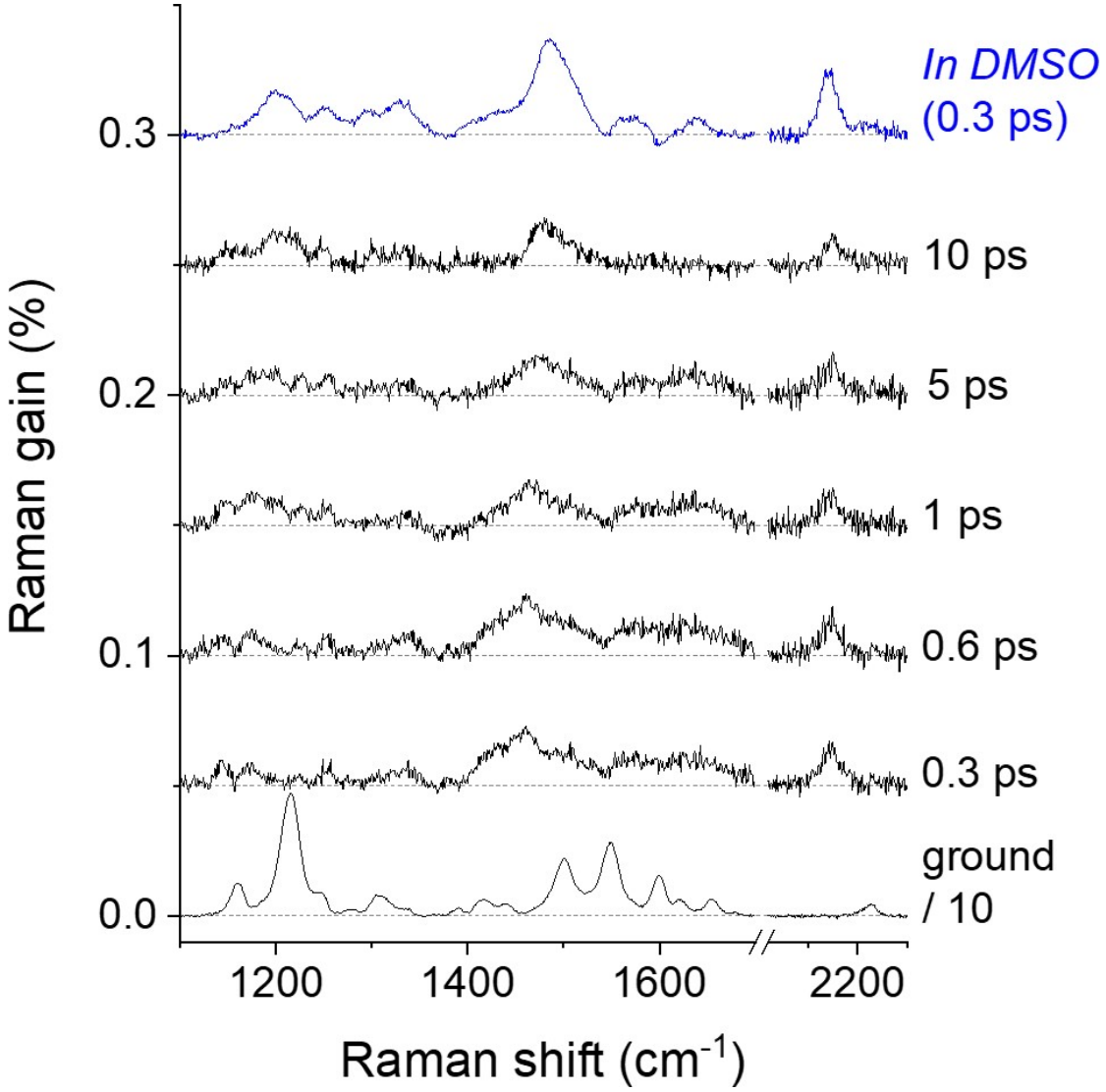

Figure S3. FSRS of LD688 in $CHCl_3$ solution obtained with 403 nm excitation. The ground-state Raman spectrum of LD688 in $CHCl_3$ solution (bottom) and the excited-state Raman spectrum of LD688 in the S_1/LE state (at 0.3 ps; top) in DMSO solution were compared.

3. DFT and TDDFT simulations of LD688

The DFT and TDDFT simulations were performed to estimate the structural changes of LD688 with the ICT using the Gaussian 09 software. The molecular geometry of LD688 in the ground state was optimized at the B3LYP/6-311G(d,p) and mPW1PBE/6-311G(d,p) levels with the PCM-DMSO for solvent effects, where LD688 appears in an overall planar geometry with the dihedral angle of the julolidine group rotation of 0.3°. Figure S5(a) shows the optimized geometry of LD688 in the ground state obtained with the DFT simulation at the B3LYP/6-311G(d,p) level.

The pseudo-potential energy curves of LD688 in DMSO along the dihedral rotation of the julolidine group were obtained by optimizing the structure of LD688 in the ground state with each fixed dihedral angle of julolidine rotation between 0 and 180° by the DFT simulation at the B3LYP/6-311G(d,p) level with PCM.[1-3] With each optimized geometry, the vertical transition energies were calculated in a single-point TDDFT simulation. The resulting potential energy curves of LD688 in the gas phase and DMSO solution were shown in Figure S4, where the potential energy curves for the ground state and the first two excited states (S_1 and S_2) were compared. The S_1 minimum (2.68 eV) was found with the twisted (dihedral angle of 90°) geometry of julolidine in the gas phase, which appears 0.07 eV lower in energy than the planar (dihedral angle of 0°; 2.75 eV) geometry. However, the S_1 minimum (2.40 eV) was found with the planar geometry in DMSO solution, which appears 0.16 eV lower in energy than the twisted geometry (2.56 eV).

Further geometry optimizations in the S_1 excited state of LD688 were performed with the initial geometries of the planar and twisted julolidine geometries obtained from the pseudo-potential curve calculations at the B3LYP/6-311G(d,p) and mPW1PBE/6-311G(d,p) levels. The optimized geometries of LD688 with the planar and twisted julolidine geometries showed slight differences

between the level of the DFT theory. In the simulation results at the B3LYP/6-311G(d,p) level of theory, the S_1 minimum (2.17 eV) was found with the planar (dihedral angle of 2.2°) geometry, which appears 0.05 eV lower in energy than the twisted (dihedral angle of 89.6°) geometry of julolidine (2.22 eV). The simulation results by the DFT methods, especially for molecules with strong charge transfer characters, can be inaccurate due to the limitation of the DFT methods.[4-5] Since the energy difference or barrier between the planar and twisted julolidine geometry estimated from the TDDFT simulations is quite small, the twisted julolidine geometry of LD688 may be considered plausible for the structural changes with the ICT in the polar medium of DMSO. Furthermore, the photoexcitation of 403 nm commonly used for transient absorption and FSRS measurements may bring some excess energy over the S_1 potential energy surface near the Franck-Condon region, which would be enough to overcome the small energy barrier between the planar and twisted julolidine geometry of LD688 in the S_1 excited state.

The optimized structures of LD688 with the planar and twisted julolidine geometry in the S_1 excited state at the B3LYP/6-311G(d,p) level were shown in Figures S5(b) and S5(c), respectively. Table S2 summarizes the TDDFT simulation results at the B3LYP/6-311G(d,p) and mPW1PBE/6-311G(d,p) levels for the optimized structures. The electron density distributions for the highest occupied molecular orbital (HOMO) and lowest unoccupied molecular orbital (LUMO) levels of LD688 obtained from the DFT simulations at the B3LYP/6-311G(d,p) level are shown in Figure S6. With the twisted julolidine geometry, the electron densities of LD688 in the HOMO and LUMO levels show distinct spatial separations between the electron-donating julolidine group and the electron-accepting dicyanomethylene moieties. The electron density distributions in the HOMO and LUMO levels strongly support the twist of the julolidine group with the ICT in the S_1 excited state.

The simulation of the Raman spectra of LD688 in the ground and excited state was also performed at various level of the DFT theory. The DFT simulations at the B3LYP/6-311G(d,p) level with the PCM-DMSO were performed for the ground-state Raman spectrum and the S_1 excited-state Raman spectra with the planar and twisted julolidine geometries in DMSO solution. The basis sets with the diffuse functions have been suggested for accurate simulation of Raman and Raman optical activity tensors.[6] The basis sets of 6-311G+(d,p) and aug(sp)-cc-pVDZ have been implemented for the simulations of the Raman spectra of LD688. The results with the 6-311G+(d,p) basis set were almost identical to those with the 6-311G(d,p) basis set, so the simulated Raman spectra with a diffuse basis set aug(sp)-cc-pVDZ are compared with those with the 6-311G(d,p) basis set. All the vibrational frequencies from the DFT simulations were rescaled by the scaling factors of 0.967 for the B3LYP/6-311G(d,p) level[7-8] and 0.963 for the B3LYP/aug(sp)-cc-pVDZ level,[9] and an appropriate bandwidth of 8 cm^{-1} was used to simulate the Raman spectra of LD688 from the frequencies and Raman intensities of the DFT simulations. Figure S7 compares the experimental and simulated ground-state Raman spectra of LD688 and DCM in DMSO solution. The vibrational assignments for the ground-state Raman spectra of LD688 were made based on the spectral similarity between the experimental and simulated results by the DFT method, summarized in Table S1. The major vibrational normal modes of LD688 in the ground state obtained from the DFT simulations were shown in Figure S8 with the vibrational assignments.

Similarly, the excited-state Raman spectra of LD688 in DMSO solution were obtained by the DFT simulations with the optimized planar and twisted julolidine geometries in the S_1 excited state. The vibrational assignments for the excited-state Raman spectra of LD688 were also made based on the spectral similarity between the experimental results and DFT simulations, both with the planar and twisted julolidine geometries. The simulated Raman spectra of LD688 in the S_1 excited

state were compared with the experimental results, as shown in Figure 4 in the manuscript. The major vibrational modes of LD688 are shown in Figure S9. Table S3 summarizes the vibrational assignments for the major vibrational modes of LD688 in the S_1 excited state.

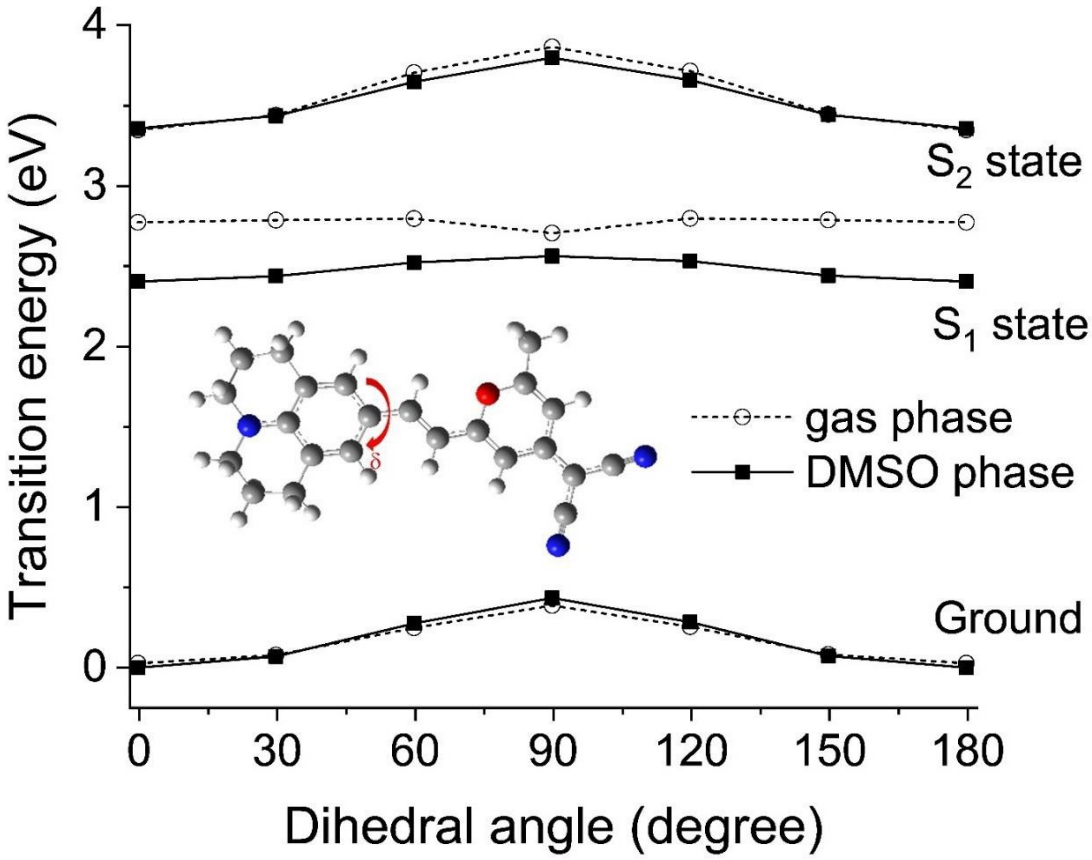

Figure S4. Pseudo-potential energy curve of LD688 in the gas phase and in DMSO solution as a function of the dihedral angle for julolidine rotation, which was obtained by the ground-state pseudo-optimization and the single point TDDFT simulations at the B3LYP/6-311G(d,p) level.

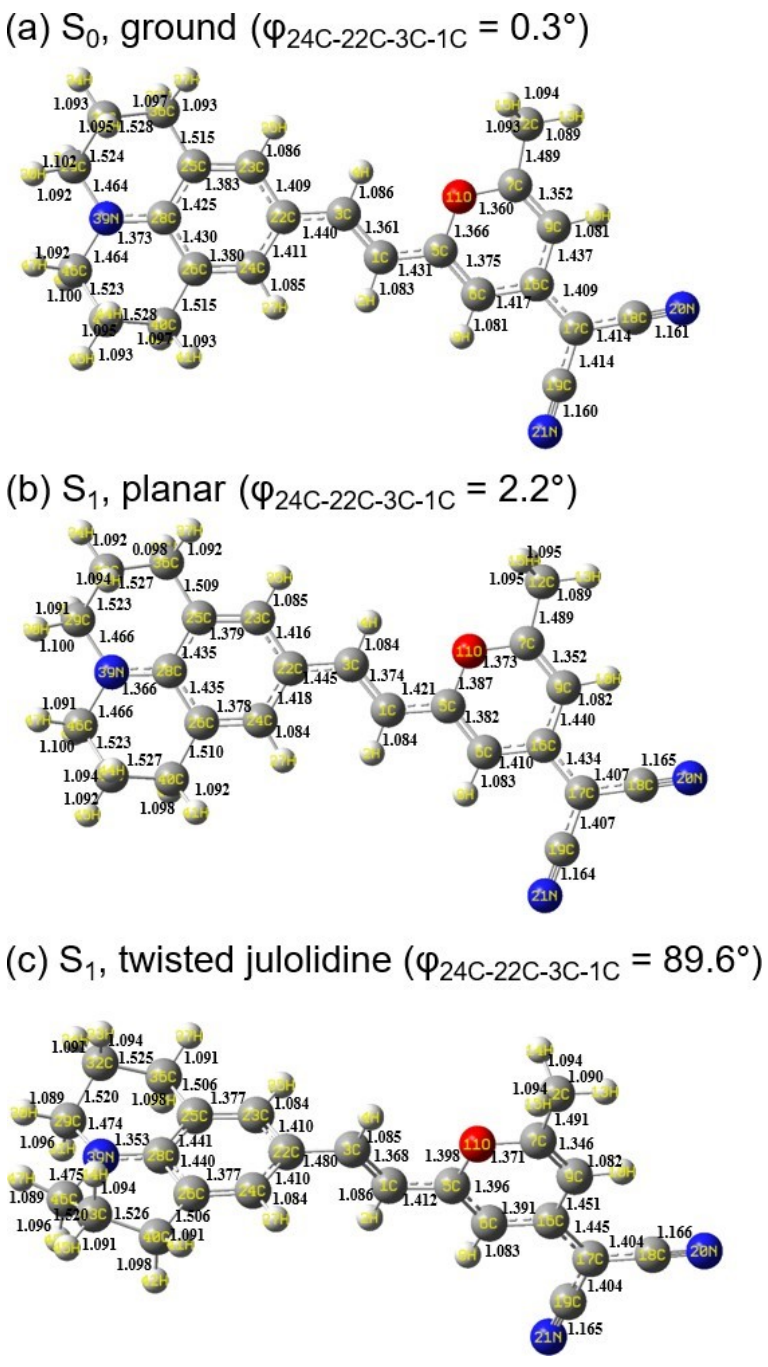

Figure S5. Optimized structures of LD688 in (a) the ground state and S_1 excited state with (b) the planar and (c) twisted julolidine group, obtained from the DFT/TDDFT simulations at the B3LYP/6-311G(d,p) levels.

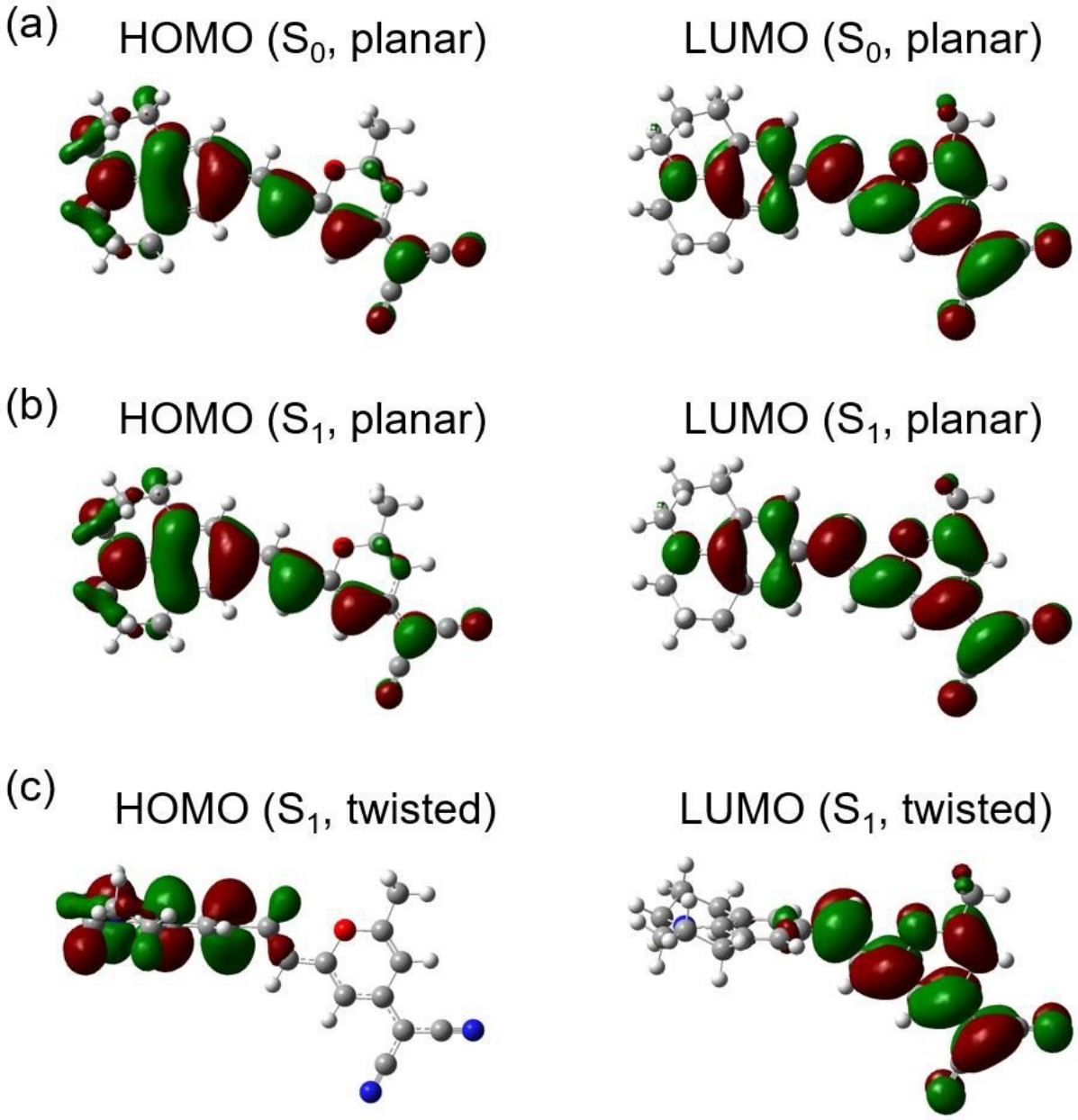

Figure S6. Frontier orbital diagrams for the highest occupied molecular orbital (HOMO) and lowest unoccupied molecular orbitals (LUMO) levels of LD688 with (a) the planar geometry in the ground state, (b) the planar, and (c) the twisted julolidine geometry in the S_1 excited state obtained from the DFT/TDDFT simulations at the B3LYP/6-311G(d,p) levels.

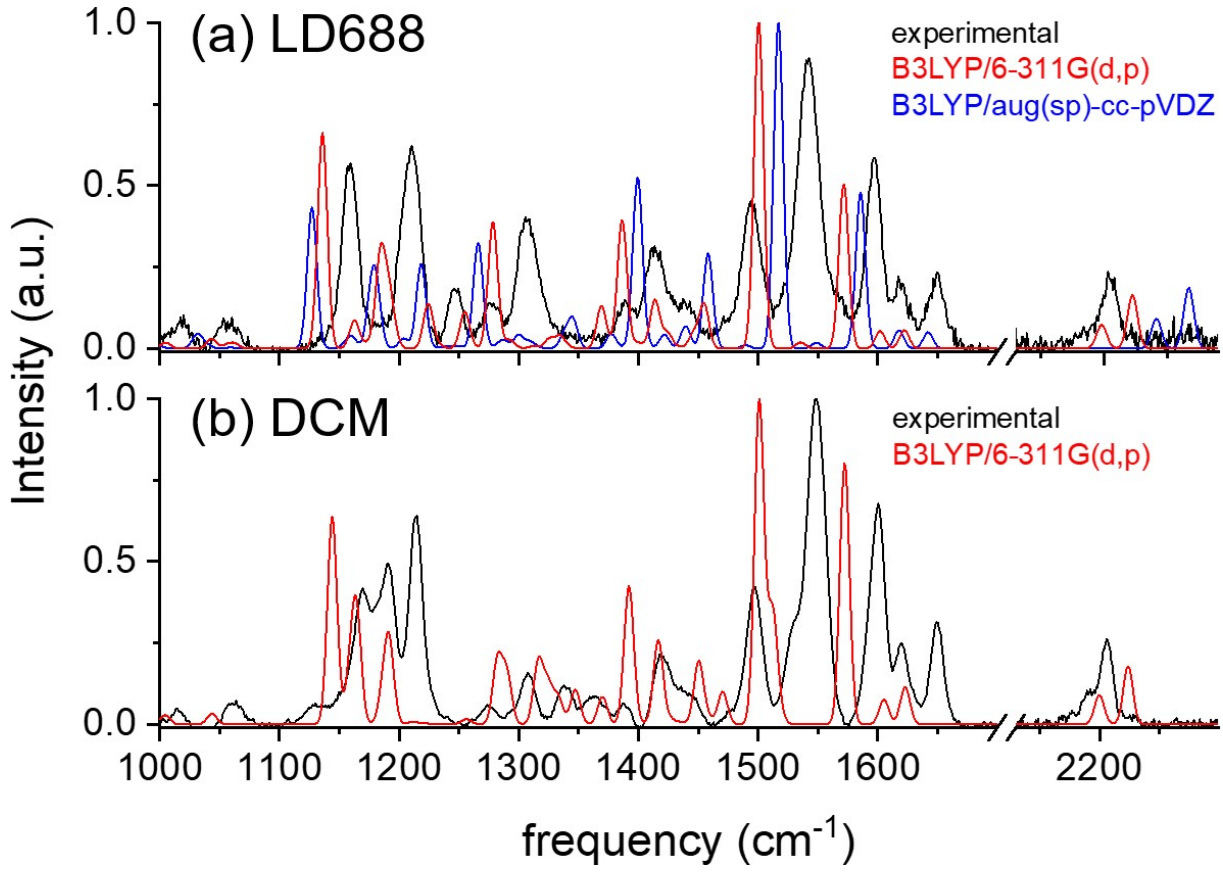

Figure S7. Ground-state (experimental) Raman spectra of (a) LD688 and (b) DCM in DMSO solution were compared with the simulated Raman spectra by the DFT methods at B3LYP/6-311G(d,p) and B3LYP/aug(sp)-cc-pVDZ levels with PCM-DMSO. The DCM spectra were adapted from ref. 1.

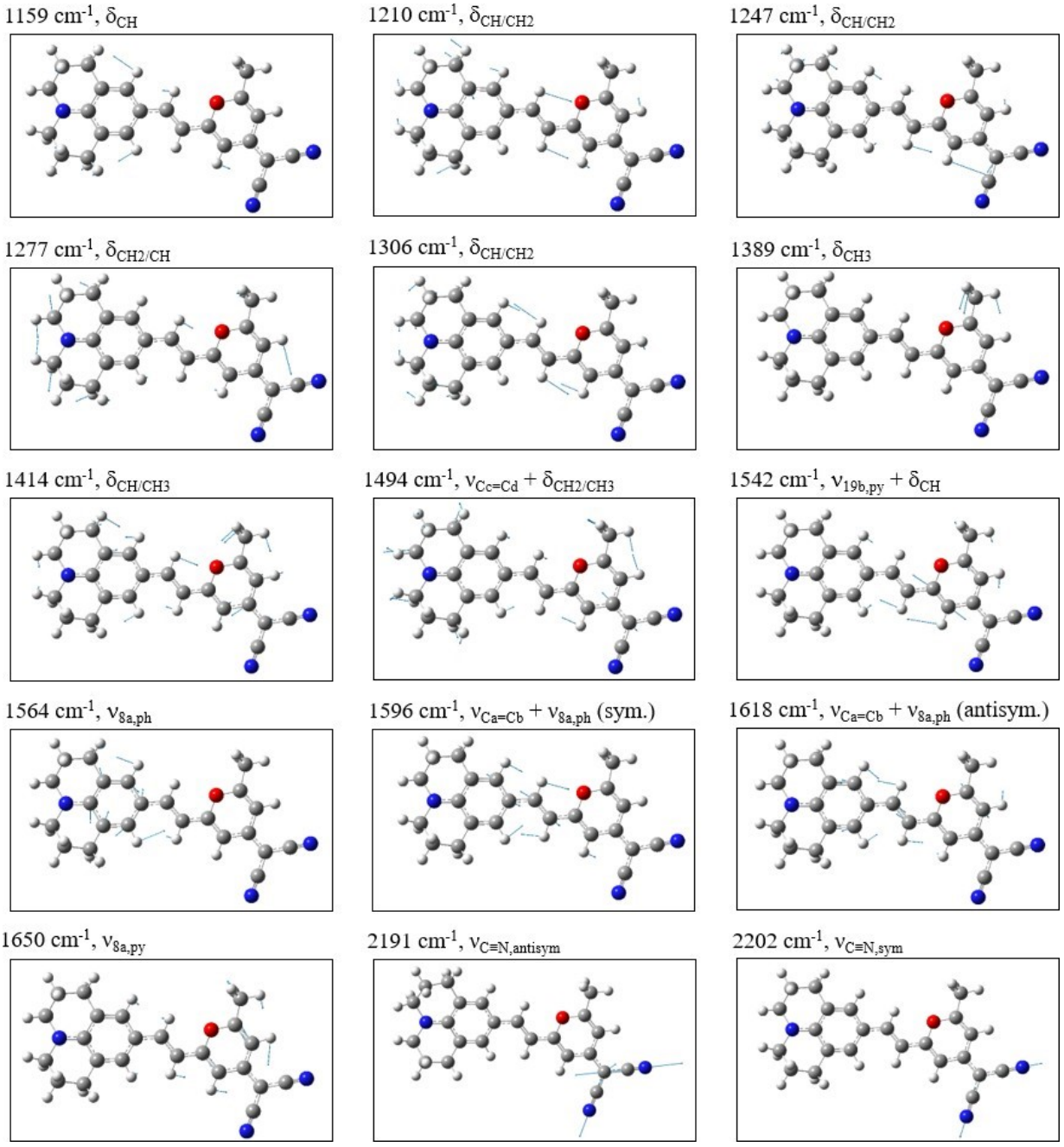

Figure S8. Vibrational normal modes of LD688 in the ground state obtained from the DFT simulations at the B3LYP/6-311G(d,p) level with PCM-DMSO. The vibrational frequencies represent the experimental values.

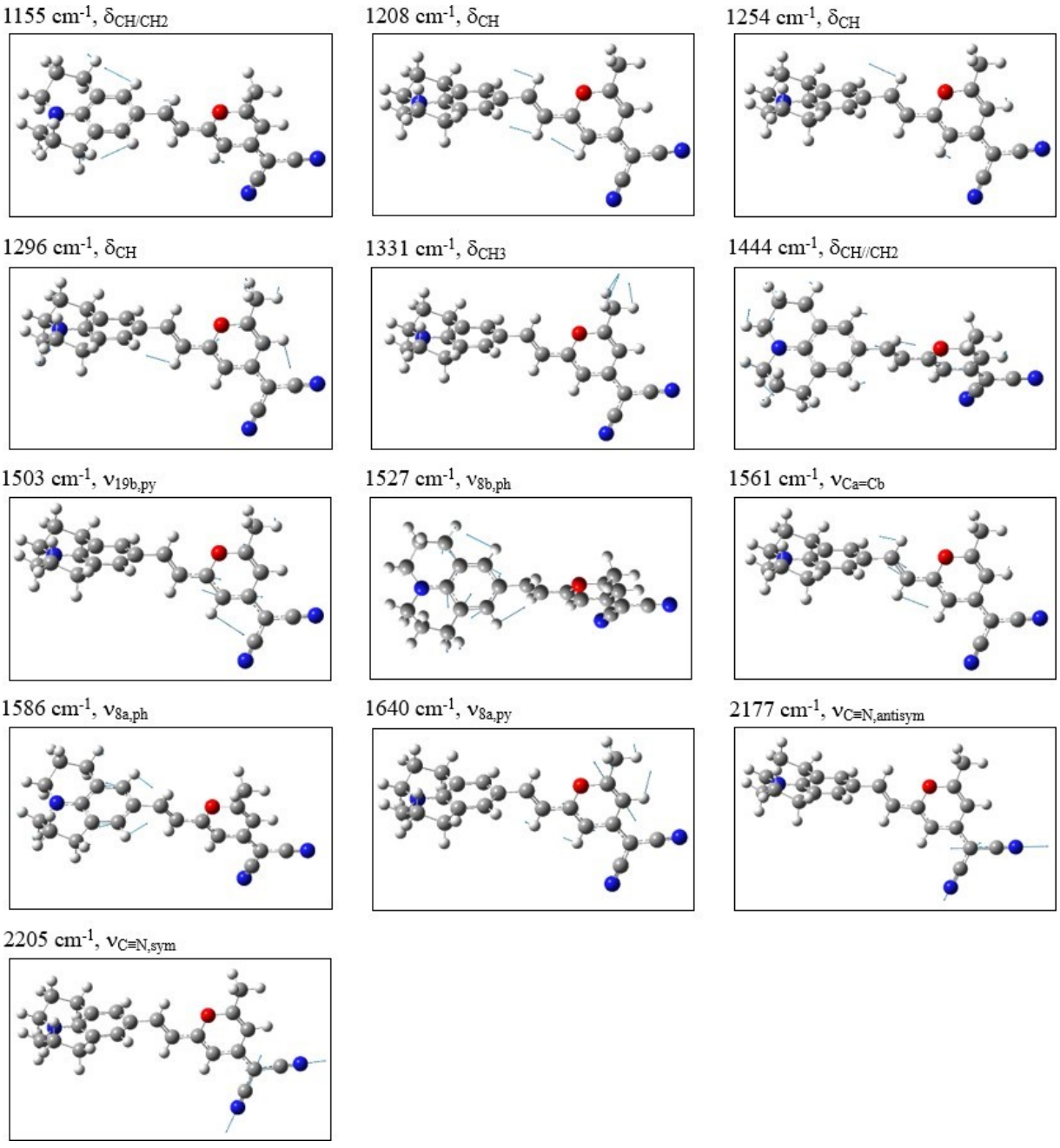

Figure S9. Vibrational normal modes of LD688 with the twisted (89.6°) julolidine geometry obtained from the TDDFT simulations at the B3LYP/6-311G(d,p) level. The vibrational frequencies represent the experimental values.

Table S1. Vibrational assignments of LD688 in the ground state

Experimental (DMSO)	Calculated [1]		Vibrational assignments [2,3]
	B3LYP/6-311G(d,p)	B3LYP/aug(sp)-cc-pVDZ	
1159	1136	1127	δ_{CH}
1210	1185	1181	$\delta_{CH/CH2}$
1247	1224	1218	$\delta_{CH/CH2}$
1277	1255	1242	$\delta_{CH2/CH}$
1306	1278	1266	$\delta_{CH/CH2}$
1389	1369	1377	δ_{CH3}
1414	1386	1400	$\delta_{CH/CH3}$
1439	1414	1407	δ_{CH3}
1494	1454	1459	$\nu_{Cc=Cd} + \delta_{CH2/CH3}$
1542	1500	1518	$\nu_{19b,py} + \delta_{CH}$
1564	1536	1549	$\nu_{8a,ph}$
1596	1572	1586	$\nu_{Ca=Cb} + \nu_{8a,ph}$ (symmetric)
1618	1602	1618	$\nu_{Ca=Cb} + \nu_{8a,ph}$ (antisymmetric)
1650	1622	1643	$\nu_{8a,py}$
2191	2198	2242	$\nu_{C\equiv N,antisym}$
2202	2222	2271	$\nu_{C\equiv N,sym}$

[1] Calculated vibrational frequencies at the B3LYP/6-311G(d,p) and B3LYP/aug(sp)-cc-pVDZ levels with a scaling factor of 0.967 and 0.963, respectively.

[2] ν and δ denote stretching and bending, respectively. The ph and py refer to the phenyl of the julolidine group and pyran ring, respectively.

[3] C_a=C_b represents the central ethylene, and C_c=C_d represents the ethylene connected to the dicyanomethylene group.

Table S2. The optimized structures of LD688 in the ground state and S_1 excited state with planar and the twisted julolidine groups

degree of freedom	ground state (S_0)	planar (S_1)	twisted julolidine (S_1)
B3LYP/6-311G(d,p) with PCM for DMSO (gas phase)			
relative energy (eV)	0.00 (0.00)	2.17 (2.69)	2.22 (2.40)
bond angle (°)			
23C-22C-3C	119.2 (119.3)	119.2 (119.6)	120.9 (121.3)
24C-22C-3C	124.0 (123.9)	123.8 (123.6)	121.0 (121.3)
22C-3C-1C	127.7 (127.6)	125.6 (124.8)	122.8 (121.9)
dihedral angle (°)			
23C-22C-3C-1C	179.5 (179.6)	177.4 (172.0)	91.1 (90.0)
24C-22C-3C-1C	0.3 (0.3)	2.2 (7.7)	89.6 (89.8)
mPW1PBE/6-311G(d,p) with PCM for DMSO			
relative energy (eV)	0.00	2.23	2.38
bond angle (°)			
23C-22C-3C	119.1	119.3	121.0
24C-22C-3C	124.0	123.9	121.0
22C-3C-1C	127.6	125.4	122.5
dihedral angle (°)			
23C-22C-3C-1C	179.5	177.6	91.1
24C-22C-3C-1C	0.3	2.0	89.4

Table S3. The vibrational frequencies and calculated vibrational frequencies of LD688 in the excited state

Experimental (in DMSO)		Calculated [1]		
LE (0.3 ps)	CT (30 ps)	Planar (2.2˚)	twisted julolidine (89.6˚)	Vibrational assignments [2, 3]
-	1155	1125 (1120)	1139 (1138)	$\delta_{CH/CH2}$
1203	1208	1182 (1178)	1185 (1175)	δ_{CH}
1252	1254	1242 (1235)	1248 (1237)	δ_{CH}
1296	1296	1294 (1282)	1302 (1296)	δ_{CH}
1329	1331	1369 (1372)	1369 (1361)	δ_{CH3}
1426	1444	1405 (1424)	1419 (1432)	$\delta_{CH/CH2}$
1485	1503	1489 (1506)	1512 (1529)	$\nu_{19b,py}$
1525	1527	1525 (1537)	1520 (1526)	$\nu_{8b,ph}$
1561	-	1547 (1559)	-	$\nu_{Ca=Cb} + \nu_{8a,ph}$ (symmetric)
-	1561	-	1572 (1589)	$\nu_{Ca=Cb}$
1586	-	1596 (1612)	-	$\nu_{Ca=Cb} + \nu_{8a,ph}$ (antisymmetric)
-	1586	-	1610 (1627)	$\nu_{8a,ph}$
1638	1640	1619 (1639)	1626 (1647)	$\nu_{8a,py}$
2170	2177	2177 (2218)	2170 (2214)	$\nu_{C\equiv N,antisym}$
2205	2205	2199 (2244)	2194 (2238)	$\nu_{C\equiv N,sym}$

[1] Calculated vibrational frequencies at the B3LYP/6-311G(d,p) and B3LYP/aug(sp)-cc-pVDZ levels with a scaling factor of 0.967 and 0.963, respectively. The frequencies outside the parentheses denote the results obtained at the B3LYP/6-311G(d,p) level and those inside the parentheses the results obtained at the B3LYP/aug(sp)-cc-pVDZ level.

[2] ν and δ denote stretching and bending, respectively. The ph and py refer to the phenyl of the julolidine group and pyran ring, respectively.

[3] C_a=C_b represents the central ethylene group.

4. References

1. Lee, S.; Jen, M.; Pang, Y., Twisted intramolecular charge transfer state of a "push-pull" emitter. *Int. J. Mol. Sci.* **2020,** *21* (21), 7999.
2. Yang, S.; Han, K., Effects of Solvent Dielectric Constant and Viscosity on Two Rotational Relaxation Paths of Excited 9-(Dicyanovinyl) Julolidine. *J. Phys. Chem. A* **2016,** *120* (27), 4961-4965.
3. Singh, C.; Ghosh, R.; Mondal, J. A.; Palit, D. K., Excited state dynamics of a push–pull stilbene: A femtosecond transient absorption spectroscopic study. *J. Photochem. Photobiol. A* **2013,** *263*, 50-60.
4. Rafiq, S.; Sen, P., Dielectric controlled excited state relaxation pathways of a representative push-pull stilbene: A mechanistic study using femtosecond fluorescence up-conversion technique. *J. Chem. Phys.* **2013,** *138* (8), 084308.
5. List, N. H.; Olsen, J. M.; Rocha-Rinza, T.; Christiansen, O.; Kongsted, J., Performance of popular XC-functionals for the description of excitation energies in GFP-like chromophore models. *Int. J. Quantum Chem* **2012,** *112* (3), 789-800.
6. Cheeseman, J. R.; Frisch, M. J., Basis Set Dependence of Vibrational Raman and Raman Optical Activity Intensities. *J Chem Theory Comput* **2011,** *7* (10), 3323-34.
7. Irikura, K. K.; Johnson, R. D.; Kacker, R. N., Uncertainties in Scaling Factors for ab Initio Vibrational Frequencies. *J. Phys. Chem. A* **2005,** *109* (37), 8430-8437.
8. Merrick, J. P.; Moran, D.; Radom, L., An Evaluation of Harmonic Vibrational Frequency Scale Factors. *J. Phys. Chem. A* **2007,** *111* (45), 11683-11700.
9. Bhattacherjee, A.; Wategaonkar, S., Conformational preferences of monohydrated clusters of imidazole derivatives revisited. *Phys. Chem. Chem. Phys.* **2015,** *17* (31), 20080-20092.